Journal of Chromatography, 4700 (1989) 21–41
Elsevier Science Publishers B.V., Amsterdam — Printed in The Netherlands

CHROM. 21 212

SEPARATION PROCESS IN ISOTACHOPHORESIS

III. TRANSIENT STATE MODELS FOR A THREE-COMPONENT SYSTEM

TAKESHI HIROKAWA*, KIYOSHI NAKAHARA and YOSHIYUKI KISO
Applied Physics and Chemistry, Faculty of Engineering, Hiroshima University, Shitami, Saijo, Higashi-hiroshima 724 (Japan)

SUMMARY

The separation of a three-component mixture (4,5-dihydroxy-3-(*p*-sulphophenylazo)-2,7-naphthalenedisulphonic acid, monochloroacetic acid and picric acid) was measured by the use of a multichannel ultraviolet-photometric zone detector. Two theoretical models which previously applied to binary systems were extended to treat the transient state of a three-component system. The formulation and the computational procedure are described in detail. Good agreement was obtained between the observed and simulated boundary velocities and resolution time, confirming the validity of the models used. Especially, the slight sample pH dependence of the resolution time was successfully simulated by one of the models (modified sample property reflecting model). The decrease in the separation capacity in the three-component system in comparison with that in the binary system was explained by the difference in the boundary velocities caused by the different potential gradients of the mixed zones.

INTRODUCTION

In isotachophoresis it is known that the resolution times for two adjacent samples in the separation of a multi-component system are always larger than those when the equivalent two samples are separated independently. As far as we know, the transient state for a three component system has not yet been simulated and the cause of the above decrease in the separation efficiency with increasing number of components in a sample has not been elucidated theoretically.

In the previous paper[1], two transient state models were proposed for the analysis of binary systems. One is based on the transient state model proposed by Mikkers *et al.*[2,3]. In this model the resolution time depends on the pH of the sample solution (pH_S) besides the pH of the leading electrolyte, the mobility of the buffer used, the mobilities and pK_a of the sample components, the migration current, etc. Since this model is sample property reflecting, we will abbreviate it as the SPR model.

According to the SPR model, the agreement between the observed and simulated

0021-9673/89/$03.50

resolution time was very good in the case of a weak acid–weak acid system, however in the case of a strong acid–weak acid system the pH_S dependence was overestimated. It was concluded that the above overestimation of the pH_S dependence was caused by the pH of the injected sample solution being perturbed by the buffer ions from the leading electrolyte at the initial stage of migration[1]. Then the SPR model was modified by considering the pH perturbation (the modified SPR model, MSPR). According to the MSPR model, the pH of the injected solution interfacing with the transient mixed zone was not kept constant after the start of the electrophoretic process. The pH shifted to higher values in anionic analysis. The shift was large enough to decrease the pH_S dependence on the separation capacity of a strong acid–weak acid system. The discrepancy between the observed and the simulated resolution time was less than 10% when the MSPR model was used[1].

The other model proposed was based on the separation diagram suggested by Brouwer and Postema[4]. In this model the separation efficiency was not affected by pH_S (non-SPR model). It was concluded that the estimation by the non-SPR model was not valid exactly, however from the practical viewpoint it cannot be denied absolutely because the simulated and the observed t_{res} agreed within *ca.* 20% not only for a weak acid–strong acid system but also a strong acid–strong acid system.

In this paper the MSPR and non-SPR models developed for binary systems were extended to treat three-component systems. To examine the validity of these models, the transient state of the system 4,5-dihydroxy-3-(*p*-sulphophenylazo)-2,7-naphthalenedisulphonic acid (SPADNS)–monochloroacetic acid (MCA)–picric acid (PIC) was observed by the use of a multi-channel UV-photometric detector[5], and the observed resolution time and the boundary velocities were compared with the theoretical estimates. The cause of the decrease in the separation efficiency of the three-component system in comparison with that of the equivalent two-component system is discussed in detail.

THEORETICAL

Fig. 1 shows the separation diagram for a three-component mixture (I) of A, B and C. Three mixed zones ABC, AB and BC are formed in the separation process. The diagram is in accord with the separation diagram for a multi-component mixture reported by Brouwer and Postema[4]. The solid lines in Fig. 1 shows the separation process in the particular case that the zone length of the injected sample solution is equal to the whole zone length at the steady state. When the concentration is high for the equivalent sample, the separation process may follow, for example, the broken lines. It was assumed that the separation diagram when the distance of the boundaries from the position of sample injection, $D >= 0$ does not depend on the sample concentration. It was revealed in the preceding paper[1] that this assumption is not strictly valid, but as already discussed it was useful as a first approximation. As revealed later, one of the practical utilities of the non-SPR model is that three mixed zones (ABC, AB and BC in Fig. 1) can be analyzed independently and therefore the time required for the iterative calculations to reach a self-consistent state is very short.

The distance, D, from the position of sample injection (the initial interface of the injected sample solution and the leading zone) was expressed as a linear function of

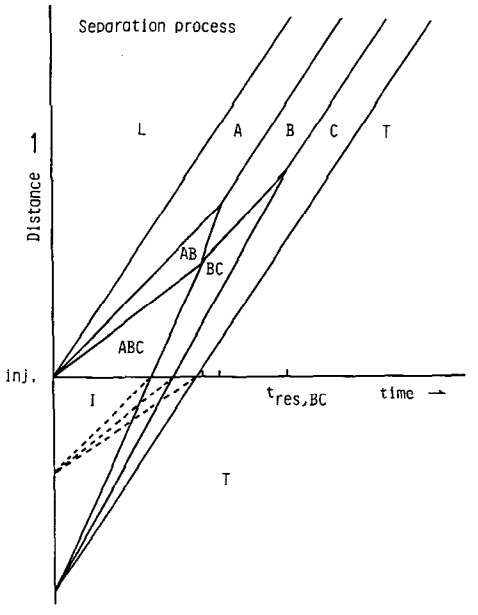

Fig. 1. Separation diagram for a three-component mixture in a separation tube. Distance = distance from injection port(inj.); time = migration time, I = zone of injected sample solution; L = leading zone; A, B and C = steady state zones; ABC, AB and BC = mixed zones; T = terminating zone and $t_{res,BC}$ = resolution time of zone BC.

time, t. We will call these linear functions the boundary functions. The separation diagram in Fig. 1 can be described by the following boundary functions

$$D_{L/A} = V_{IP}t \quad (1)$$
$$D_{A/B} = V_{IP}t - l_A \quad (2)$$
$$D_{B/C} = V_{IP}t - (l_A + l_B) \quad (3)$$
$$D_{C/T} = V_{IP}t - (l_A + l_B + l_C) \quad (4)$$
$$D_{A/AB} = V_{A/AB}t \quad (5)$$
$$D_{AB/B} = V_{AB/B}t - D_{0,AB/B} \quad (6)$$
$$D_{B/BC} = V_{B/BC}t - D_{0,B/BC} \quad (7)$$
$$D_{BC/C} = V_{BC/C}t - D_{0,BC/C} \quad (8)$$
$$D_{AB/ABC} = V_{AB/ABC}t \quad (9)$$
$$D_{ABC/BC} = V_{ABC/BC}t - (l_A + l_B + l_C) \quad (10)$$

where AB, BC and ABC denote the mixed zones, V_{IP} the isotachophoretic velocity, V the velocity of the boundary, D_0 the intercepts of the boundary function and l_A, l_B and l_C are the zone lengths of the components at the steady state, which vary in proportion to the sample amounts.

The velocities of the mixed zone boundaries can be derived from the moving boundary equation[6] as

$$V_{A/AB} = E_{AB}\bar{m}_{B,AB} \quad (11)$$
$$V_{AB/B} = E_{AB}\bar{m}_{A,AB} \quad (12)$$
$$V_{B/BC} = E_{BC}\bar{m}_{C,BC} \quad (13)$$
$$V_{BC/C} = E_{BC}\bar{m}_{B,BC} \quad (14)$$
$$V_{AB/ABC} = E_{ABC}\bar{m}_{C,ABC} \quad (15)$$
$$V_{ABC/BC} = E_{ABC}\bar{m}_{A,ABC} \quad (16)$$

where E denotes the potential gradient of the mixed zone and $\bar{m}$ the effective mobility of the sample components in the mixed zone, for example, $\bar{m}_{A,ABC}$ is the effective mobility of A in the mixed zone ABC.

Non-SPR model for three-component system

This model directly depends on the separation diagram shown in Fig. 1: the total amount of samples in the zone interposed by the boundaries L/A and C/T equals the injected amount, and is constant regardless of whether the separation process is at the transient state or at the steady state. It should be noted that both the non-SPR and the MSPR models utilize the effective mobilities of samples and the buffer, the concentration and the zone length at the steady state. These can be simulated exactly as reported previously[7,8].

Mixed zone ABC. Relationships between the sample concentrations of the steady state zones, $C^t_{A,S}$, $C^t_{B,S}$ and $C^t_{C,S}$, and those of the mixed zone ABC can be derived, which are closely related with t_{res}:

$$C^t_{A,ABC} = l_A/(l_A + l_B + l_C)C^t_{A,S} \quad (17)$$
$$C^t_{B,ABC} = l_B/(l_A + l_B + l_C)C^t_{B,S} \quad (18)$$
$$C^t_{C,ABC} = l_C/(l_A + l_B + l_C)C^t_{C,S} \quad (19)$$

The concentration of the buffer ion in the mixed zone ABC can be expressed as

$$C^t_{Q,ABC} = (l_A C^t_{Q,A} + l_B C^t_{Q,B} + l_C C^t_{Q,C})/(l_A + l_B + l_C) \quad (20)$$

where $C^t_{Q,A}$, $C^t_{Q,B}$ and $C^t_{Q,C}$ denote the buffer concentrations in the steady state zones, A, B and C.

On the other hand, resolution time of the mixed zone ABC is obtained by solving the simultaneous eqns. 9, 10, 15 and 16:

$$t_{res,ABC} = (l_A + l_B + l_C)/[E_{ABC}(m_{A,ABC} - m_{C,ABC})] \quad (21)$$

The iterative calculations to fulfil the electrophoretic conditions were as follows.

(1) l_A, l_B, l_C, $C^t_{A,S}$, $C^t_{B,S}$, $C^t_{C,S}$, $C^t_{Q,A}$, $C^t_{Q,B}$ and $C^t_{Q,C}$ were evaluated from the steady state analysis[7,8].

(2) The mobilities of the sample components A, B and C and the buffer ion Q were calculated on the basis of the dissociation constants and the pH of the mixed zone. In the first stage of iteration, the pH of the zone ABC(pH_{ABC}) was assumed equal to the pH of the leading electrolyte (pH_L). The correction for ionic strength was considered for the mobilities and acid dissociation constants throughout the present simulation.

(3) $C^{\P}_{A,ABC}$, $C^{\P}_{B,ABC}$ and $C^{\P}_{C,ABC}$ were evaluated by use of eqns. 17–19. The partial concentrations of the component ions at pH_{ABC} were also calculated.

(4) $C^{\P}_{Q,ABC}$ was calculated on the basis of the electroneutrality principle ($C^{\P}_{Q,ABC} \equiv$ CTQ1).

(5) $C^{\P}_{Q,ABC}$ was calculated by use of eqn. 20 ($\equiv$ CTQ2). The partial concentration of the buffer ion at pH_{ABC} was calculated from CTQ2.

(6) The specific conductivity of the mixed zone, κ_{ABC}, was calculated considering all ionic constituents.

(7) The potential gradient of the zone ABC(E_{ABC}) was calculated by the use of κ_{ABC} and the migration current.

(8) CTQ1 should be equal to CTQ2. The consistency was checked by use of the following RFC function:

$$RFC = (CTQ1/CTQ2) - 1 \tag{22}$$

Until RFC was considered as zero (actually we used a threshold value of 10^{-5}), steps 1–8 were repeated, varying the pH of the mixed zone. The right direction of the pH change was judged by the change of |RFC|.

Mixed zone AB. Instead of eqn. 20 for the mixed zone ABC, the total concentration of the buffer ion in the mixed zone, $C^{\P}_{Q,AB}$, was calculated from the following equation derived from the moving boundary equation[6] for the boundary A/AB:

$$C^{\P}_{Q,AB} = \frac{\bar{m}_{Q,A}E_A + \bar{m}_{B,AB}E_{AB}}{(\bar{m}_{Q,AB} + \bar{m}_{B,AB})E_{AB}} \cdot C^{\P}_{Q,A} \tag{23}$$

The potential gradient, E_{AB}, was also derived from the moving boundary equation:

$$E_{AB} = \frac{\bar{m}_A C^{\P}_A}{\bar{m}_{A,AB}C^{\P}_{A,AB} + \bar{m}_{B,AB}(C^{\P}_A - C^{\P}_{A,AB})} \cdot E_A \tag{24}$$

The total concentrations of the components A and B can be expressed as follows by applying the moving boundary equation to the boundary AB/ABC:

$$C^{\P}_{A,AB} = \frac{(\bar{m}_{A,ABC} - \bar{m}_{C,ABC})E_{ABC}}{\bar{m}_{A,AB}E_{AB} - \bar{m}_{C,ABC}E_{ABC}} \cdot C^{\P}_{A,ABC} \tag{25}$$

$$C^{\P}_{B,AB} = \frac{(\bar{m}_{B,ABC} - \bar{m}_{C,ABC})E_{ABC}}{\bar{m}_{B,AB}E_{AB} - \bar{m}_{C,ABC}E_{ABC}} \cdot C^{\P}_{B,ABC} \tag{26}$$

The resolution time, $t_{res,AB}$, can be expressed as in the binary system using eqns. 2 and 5:

$$t_{res,AB} = l_A/(V_{IP} - V_{A/AB}) \tag{27}$$

The iterative calculations for the mixed zone AB were performed as follows.

(1) The mobilities of the sample components A, B and C and the buffer ion

Q were calculated on the basis of the dissociation constants and the pH of the mixed zone. In the first stage of iteration, the pH of the zone AB(pH_{AB}) was assumed equal to pH_{ABC}.

(2) $C^t_{Q,AB}$ was calculated by use of eqn. 23 ($\equiv$ CTQ3). The partial concentration of the buffer ion at pH_{AB} was calculated from CTQ3.

(3) The potential gradient of the zone AB(E_{AB}) was calculated by the use of eqn. 24.

(4) $C^t_{A,AB}$ and $C^t_{B,AB}$ were evaluated by use of eqns. 25 and 26. The partial concentrations of the component ions at pH_{AB} were also calculated.

(5) $C^t_{Q,AB}$ was calculated on the basis of the electroneutrality principle ($C^t_{Q,AB} \equiv$ CTQ4).

(6) CTQ3 should be equal to CTQ4. The consistency was checked by use of the following RFC function:

$$RFC = (CTQ3/CTQ4) - 1 \tag{28}$$

Until RFC was considered as zero (actually we used a threshold value of 10^{-5}), steps 1–6 were repeated, varying the pH of the mixed zone.

Mixed zone BC. The moving boundary equation[6] was adopted for the boundary BC/C, the following expression for the total concentration of buffer being derived:

$$C^t_{Q,BC} = \frac{\bar{m}_{Q,C}E_C + \bar{m}_{B,BC}E_{BC}}{(\bar{m}_{Q,BC} + \bar{m}_{B,BC})E_{BC}} \cdot C^t_{Q,C} \tag{29}$$

The potential gradient, E_{BC}, is given by:

$$E_{BC} = \frac{\bar{m}_C E_C C^t_C}{\bar{m}_{C,BC}C^t_{C,BC} + \bar{m}_{B,BC}(C^t_C - C^t_{C,BC})} \tag{30}$$

The total concentration of the components B and C can be expressed as follows by applying the moving boundary equation to the boundary ABC/AB:

$$C^t_{B,BC} = \frac{(\bar{m}_{A,ABC} - \bar{m}_{B,ABC})E_{ABC}}{\bar{m}_{A,ABC}E_{ABC} - \bar{m}_{B,BC}E_{BC}} \cdot C^t_{B,ABC} \tag{31}$$

$$C^t_{C,BC} = \frac{(\bar{m}_{A,ABC} - \bar{m}_{C,ABC})E_{ABC}}{\bar{m}_{A,ABC}E_{ABC} - \bar{m}_{C,BC}E_{BC}} \cdot C^t_{C,ABC} \tag{32}$$

The resolution time, $t_{res,BC}$, may be expressed as follows:

$$t_{res,BC} = l_C/(V_{BC/C} - V_{IP}) \tag{33}$$

The iteration was carried as described for the mixed zone AB.

MSPR model for three-component system

This model does not utilize eqns. 17–20 to express the concentration of the zone constituents. Instead, the moving boundary equation[6] was adopted for the boundary between the injected sample solution and the mixed zone ABC on the assumption that the boundary is solvent-fixed. The formulation and the iterative calculation were somewhat complex, a more exact simulation was expected in comparison with the non-SPR model.

In the MSPR model, a zone (I*) of which the pH is different from the pH_S is considered between the injection position and the boundary moving with velocity $E_I m_{Q,I}$(E_I = the potential gradient of the injected solution and $m_{Q,I}$ the effective mobility of the buffer ion)[1]. The pH perturbation was caused by the counter ion from the leading electrolyte. On the assumption that the velocity of the boundary I*/ABC is zero, the concentration of the counter ions in the zone I*, $C^t_{Q,I}$*, can be written as follows from the continuity principle

$$C^t_{Q,I}{}^* = E_I \bar{m}_{Q,L} C^t_{Q,I} / E_I \bar{m}_{Q,I} + C^t_{Q,I} \tag{34}$$

where E_L denotes the potential gradient of the leading zone, $\bar{m}_{Q,L}$ the effective mobility of buffer ions in the leading zone and $C^t_{Q,L}$ and $C^t_{Q,I}$ the total concentration of buffer in the leading zone and in the initial sample solution respectively. Although the sample concentrations in the zone I* are equal to those of the injected sample solution, the potential gradient and effective mobilities are different from those in the injected solution.

Mixed zone ABC. On the assumption that the boundary I*/ABC is an ideal concentration boundary, namely the boundary velocity is zero, one can obtain the following equations to correlate the concentrations of the sample solution and those of the mixed zone

$$E_I{}^* \bar{m}_{A,I}{}^* C^t_{A,I}{}^* = E_{ABC} \bar{m}_{A,ABC} C^t_{A,ABC} \tag{35}$$

$$E_I{}^* \bar{m}_{B,I}{}^* C^t_{B,I}{}^* = E_{ABC} \bar{m}_{B,ABC} C^t_{B,ABC} \tag{36}$$

$$E_I{}^* \bar{m}_{C,I}{}^* C^t_{C,I}{}^* = E_{ABC} \bar{m}_{C,ABC} C^t_{C,ABC} \tag{37}$$

where E_I* is the potential gradient of the zone (I*) actually interfacing the mixed zone ABC, $\bar{m}_{A,I}$*,$\bar{m}_{B,I}$* and $\bar{m}_{C,I}$* the effective mobilities in the zone and $C^t_{A,I}$*, $C^t_{B,I}$* and $C^t_{C,I}$* the total concentrations in the zone. Hereafter I* is abbreviated as I for convenience. From these equations the ratios of the sample concentrations in the zone ABC can be expressed as:

$$\frac{C^t_{B,ABC}}{C^t_{A,ABC}} = \frac{\bar{m}_{A,ABC} \bar{m}_{B,I} C^t_{B,I}}{\bar{m}_{B,ABC} \bar{m}_{A,I} C^t_{A,I}} \equiv F_5 \tag{38}$$

$$\frac{C^t_{C,ABC}}{C^t_{A,ABC}} = \frac{\bar{m}_{A,ABC} \bar{m}_{C,I} C^t_{C,I}}{\bar{m}_{C,ABC} \bar{m}_{A,I} C^t_{A,I}} \equiv F_6 \tag{39}$$

From the electroneutrality relationship in the mixed zone, the concentrations of components A, B and C can be calculated

$$C^{t}_{A,ABC} = F_1/(F_2 + F_3F_5 + F_4F_6) \tag{40}$$

$$C^{t}_{B,ABC} = C^{t}_{A,ABC}F_5 \tag{41}$$

$$C^{t}_{C,ABC} = C^{t}_{A,ABC}F_6 \tag{42}$$

$$F_1 = -[C_H - C_{OH} + C^{t}_{Q,ABC}/(1 + k_Q/C_H)] \tag{43}$$

$$F_2 = \frac{\sum_{i=1}^{n_A}\left[z_{A,i}\left(\prod_i k_{A,i}\right)\Big/ C_H^i\right]}{1 + \sum_{i=1}^{n_A}\left(\prod_i k_{A,i}\right)\Big/ C_H^i} \tag{44}$$

$$F_3 = \frac{\sum_{i=1}^{n_B}\left[z_{B,i}\left(\prod_i k_{B,i}\right)\Big/ C_H^i\right]}{1 + \sum_{i=1}^{n_B}\left(\prod_i k_{B,i}\right)\Big/ C_H^i} \tag{45}$$

$$F_4 = \frac{\sum_{i=1}^{n_C}\left[z_{C,i}\left(\prod_i k_{C,i}\right)\Big/ C_H^i\right]}{1 + \sum_{i=1}^{n_C}\left(\prod_i k_{C,i}\right)\Big/ C_H^i} \tag{46}$$

where C_H and C_{OH} denote the concentration of H^+ and OH^-, $C^{t}_{Q,ABC}$ the total concentration of buffer in the zone ABC, k_Q, k_A, k_B and k_C the acid dissociation constants, $z_{A,i}$, $z_{B,i}$ and $z_{C,i}$ the ionic charge of the ith dissociated ion of the components A, B and C and n_A, n_B and n_C the numbers of the constituent ionic species. The monovalent cationic buffer was assumed in eqn. 43.

On the other hand, the following relationship is obtained between the buffer concentration of the mixed zone AB and that of the mixed zone ABC by applying the moving boundary equation to the boundary AB/ABC:

$$C^{t}_{Q,AB} = \frac{(\bar{m}_{C,ABC} + \bar{m}_{Q,ABC})E_{ABC}}{\bar{m}_{C,ABC}E_{ABC} + \bar{m}_{Q,AB}E_{AB}} \cdot C^{t}_{Q,ABC} \tag{47}$$

By combining eqns. 23 and 47, one obtains a relationship between the buffer concentration of the mixed zone ABC and that of the zone A at the steady state:

$$C^{t}_{Q,ABC} = \frac{(\bar{m}_{C,ABC}E_{ABC} + \bar{m}_{Q,AB}E_{AB})(\bar{m}_{Q,A}E_A + \bar{m}_{B,AB}E_{AB})}{(\bar{m}_{C,ABC} + \bar{m}_{Q,ABC})E_{ABC}(\bar{m}_{Q,AB} + \bar{m}_{B,AB})E_{AB}} \cdot C^{t}_{Q,A} \tag{48}$$

The potential gradient of the zone ABC(E_{ABC}) in eqn. 48 can be estimated by the following equations which correlate E_{ABC} and E_A:

$$E_{ABC} = \bar{m}_A C^t_A \bar{m}_{A,AB} C^t_{A,AB} E_A/(F_7 F_8) \tag{49}$$

$$F_7 = \bar{m}_{B,AB} C^t_A + (\bar{m}_{A,AB} - \bar{m}_{B,AB}) C^t_{A,AB} \tag{50}$$

$$F_8 = \bar{m}_{C,ABC} C^t_{A,AB} + (\bar{m}_{A,ABC} - \bar{m}_{C,ABC}) C^t_{A,ABC} \tag{51}$$

Eqns. 48 and 49 contain E_{AB}, $\bar{m}_{A,AB}$ and $\bar{m}_{B,AB}$ suggesting that the mixed zone ABC cannot be analyzed independently, in contrast to the non-SPR model.

Mixed zone AB. From eqns. 25 and 35, the concentration of component A of the mixed zone AB can be correlated with that of the injected solution. The concentration of component B can be correlated in a similar manner. Accordingly the ratio of the sample concentrations can be expressed as follows:

$$\frac{C^t_{B,AB}}{C^t_{A,AB}} = \frac{F_9 \bar{m}_{A,AB} \bar{m}_{B,I} C^t_{B,I}}{F_{10} \bar{m}_{B,AB} \bar{m}_{A,I} C^t_{A,I}} \tag{52}$$

$$F_9 = \frac{(\bar{m}_{C,ABC} - \bar{m}_{B,ABC})}{\bar{m}_{C,ABC} E_{ABC} - \bar{m}_{B,AB} E_{AB}} \tag{53}$$

$$F_{10} = \frac{(\bar{m}_{C,ABC} - \bar{m}_{A,ABC})}{\bar{m}_{C,ABC} E_{ABC} - \bar{m}_{A,AB} E_{AB}} \tag{54}$$

In case of the binary system, F_9 and F_{10} in eqn. 52 are unity. Eqn. 52 contains the effective mobilities of the components A, B and C in the zone ABC and the potential gradient. Thus the zones ABC and AB should be analyzed simultaneously. The buffer concentration and the potential gradient of the zone AB can be correlated with those of the zone A as shown in eqns. 23 and 24.

Mixed zone BC. From the moving boundary equations for boundary ABC/BC, the concentration ratio of the components B and C can be expressed as follows:

$$\frac{C^t_{C,BC}}{C^t_{B,BC}} = \frac{F_{11} C^t_{C,ABC}}{F_{12} C^t_{B,ABC}} \tag{55}$$

$$F_{11} = \frac{(\bar{m}_{C,ABC} - \bar{m}_{A,ABC}) E_{ABC}}{\bar{m}_{C,BC} E_{BC} - \bar{m}_{A,ABC} E_{ABC}} \tag{56}$$

$$F_{12} = \frac{(\bar{m}_{B,ABC} - \bar{m}_{A,ABC}) E_{ABC}}{\bar{m}_{B,BC} E_{BC} - \bar{m}_{A,ABC} E_{ABC}} \tag{57}$$

The concentration of buffer can be expressed as:

$$C^t_{Q,BC} = \frac{(\bar{m}_{Q,ABC} + \bar{m}_{A,ABC}) E_{ABC}}{\bar{m}_{Q,BC} E_{BC} + \bar{m}_{A,ABC} E_{ABC}} \cdot C^t_{Q,ABC} \tag{58}$$

The potential gradient, E_{BC}, is correlated with E_{ABC} as:

$$E_{BC} = \frac{(\bar{m}_{B,ABC} - \bar{m}_{A,ABC})C^{t}_{B,ABC} + \bar{m}_{A,ABC}C^{t}_{B,BC}}{C^{t}_{B,BC}\bar{m}_{B,BC}} \cdot E_{ABC} \tag{59}$$

Thus in the MSPR model, even if the sample amount is constant, the properties of the mixed zone (the pH, the total concentration of the constituents, the effective mobilities, the potential gradient) depend on the pH_S, therefore the resolution time depends on pH_S. This dependence is remarkable in that weak electrolytes are contained in the sample system.

As mentioned before, the properties of the mixed zones ABC, AB and BC are correlated with each other; they cannot be analyzed independently in contrast to the case of the non-SPR model. By the use of the present formulation, at least the zones ABC and AB can be treated at once. The iterative calculations to reach the self-consistent state using the above equations are as follows.

(1) l_A, l_B, l_C, $C^{t}_{A,S}$, $C^{t}_{B,S}$, $C^{t}_{C,S}$, $C^{t}_{Q,A}$, $C^{t}_{Q,B}$ and $C^{t}_{Q,C}$ were evaluated from the steady state analysis[7,8]. The pH, potential gradient, the effective mobilities in the zone I* were evaluated by iterative calculation so as to fulfil eqn. 34.

(2) The zone AB was analyzed using the MSPR model for a binary system to give appropriate initial values in the subsequent iterative calculation. This process is decisive for the smooth convergence of the iteration.

(3) The zone ABC was first treated. The effective mobilities of the sample components A, B and C and the buffer ion Q were calculated on the basis of the dissociation constants and the pH of the mixed zone. In the first stage of iteration, the pH of the zone ABC(pH_{ABC}) was assumed being equal to the averaged pH of the steady state zones.

(4) The potential gradient of the zone ABC(E_{ABC}) was calculated by the use of eqn. 49. In the first stage of the iteration, E_{AB} and the effective mobilities in the zone AB were those estimated in the above step (2).

(5) $C^{t}_{Q,ABC}$ was calculated by use of eqn. 48. The partial concentration of the buffer ion at pH_{ABC} was also calculated.

(6) $C^{t}_{A,ABC}$, $C^{t}_{B,ABC}$ and $C^{t}_{C,ABC}$ were evaluated from the electro neutrality relationship using eqns. 40–46. The partial concentrations of the component ions at pH_{ABC} were also calculated.

(7) The specific conductivity of the mixed zone, κ_{ABC}, was calculated considering all ionic constituents.

(8) The consistency of the current density was checked by use of the following RFQ function

$$RFQ_{ABC} = (E_{ABC}\kappa_{ABC}/E_L\kappa_L) - 1 \tag{60}$$

where E_L and κ_L denote the potential gradient and the specific conductivity of the leading zone. In the first stage of iteration RFQ_{ABC} was never zero, since E_{AB} and the effective mobilities in the zone AB were the assumed values. To decrease $|RFQ_{ABC}|$, more appropriate values were necessary.

(9) Then the zone AB was treated. The effective mobilities of the samples and the

buffer were calculated at the pH of the mixed zone (pH_{AB}). In the first stage of iteration, pH_{AB} was assumed equal to that estimated in step (2).

(10) The potential gradient, E_{AB}, was calculated by eqn. 24.

(11) $C^t_{Q,AB}$ was calculated by use of eqn. 23.

(12) $C^t_{A,AB}$ and $C^t_{B,AB}$ were evaluated from the electroneutrality relationship on the basis of the concentration ratio (eqn. 52).

(13) The specific conductivity of the mixed zone, κ_{AB}, was calculated considering all ionic constituents.

(14) The iterative calculation, steps (9)–(13), was carried until the following RFQ function was zero on varying pH_{AB}:

$$RFQ_{AB} = (E_{AB}\kappa_{AB}/E_L\kappa_L) - 1 \tag{61}$$

Unless the estimated properties of the zone ABC were extremely wrong, the iterative calculation converged within 30 cycles.

(15) After the convergence of RFQ_{AB}, the new values of E_{AB} and the effective mobilities were obtained. Using these values, steps (3)–(14) were repeated varying pH_{ABC} until $|RFQ_{ABC}|$ was less than 10^{-5}. When pH_{ABC} and pH_{AB} were determined, all properties of the zones ABC and AB were obtained simultaneously.

(16) Last, the zone BC was treated. The effective mobilities of the samples and the buffer were calculated at the pH of the mixed zone (pH_{BC}). In the first stage of iteration, pH_{BC} was assumed equal to pH_{AB}.

(17) The potential gradient, E_{BC}, was obtained by use of eqn. 59.

(18) $C^t_{Q,BC}$ was calculated by use of eqn. 58.

(19) $C^t_{B,BC}$ and $C^t_{C,BC}$ were evaluated from the electroneutrality relationship on the basis of the concentration ratio (eqn. 55).

(20) The specific conductivity of the mixed zone, κ_{BC}, was calculated considering all ionic constituents.

(21) The iterative calculation, steps (16)–(21), was carried out until the following RFQ function was regarded as zero upon varying pH_{BC}:

$$RFQ_{BC} = (E_{BC}\kappa_{BC}/E_L\kappa_L) - 1 \tag{62}$$

Thus all mixed zones were analyzed successfully. It should be noted that RFQ_{ABC} and RFQ_{AB} have to be zero simultaneously.

The resolution time of the mixed zone AB($t_{res,AB}$) can be expressed by eqn. 27. However, in the MSPR model, t_{res} of the mixed zones ABC and BC were not expressed by eqns. 21 and 33, because the equations were derived from the separation diagram in Fig. 1 on the assumptions that the intercepts of the boundary functions of ABC/BC, BC/C and C/T coincide with each other. Once $t_{res,AB}$ was evaluated, the boundary function of AB/B (eqn. 6) can be expressed as follows:

$$D_{AB/B} = \bar{m}_{A,AB}E_{AB}t - (\bar{m}_{A,AB} - \bar{m}_{B,AB})E_{AB}t_{res,AB} \tag{6'}$$

Using eqns. 6′ and 9, one can obtain $t_{res,ABC}$ without use of the above assumption as follows:

$$t_{res,ABC} = \frac{(\bar{m}_{B,AB} - \bar{m}_{A,AB})E_{AB}t_{res,AB}}{\bar{m}_{C,ABC}E_{ABC} - \bar{m}_{A,AB}E_{AB}} \tag{63}$$

Similarly, the boundary function of B/BC (eqn. 7) can be expressed using $t_{res,ABC}$ as follows:

$$D_{B/BC} = \bar{m}_{C,BC}E_{BC}t - (\bar{m}_{C,BC}E_{BC} - \bar{m}_{C,ABC}E_{ABC})t_{res,ABC} \tag{7'}$$

Then $t_{res,BC}$ can be defined as the time when the difference of the distances between eqn. 7′ and eqn. 2 for the boundary A/B equals the steady state zone length, l_B:

$$t_{res,BC} = \frac{l_A + l_B + (\bar{m}_{C,ABC}E_{ABC} - \bar{m}_{C,BC}E_{BC})t_{res,ABC}}{V_{IP} - \bar{m}_{C,BC}E_{BC}} \tag{64}$$

The boundary functions of BC/C and ABC/BC can be expressed as follows:

$$D_{BC/C} = \bar{m}_{B,BC}E_{BC}t - [(\bar{m}_{B,BC} - \bar{m}_{C,BC})E_{BC}t_{res,BC} + \\ + (\bar{m}_{C,BC}E_{BC} - \bar{m}_{C,ABC}E_{ABC})t_{res,ABC}] \tag{8'}$$

$$D_{ABC/BC} = \bar{m}_{A,ABC}E_{ABC}t - (\bar{m}_{A,ABC} - \bar{m}_{C,ABC})E_{ABC}t_{res,ABC} \tag{10'}$$

Using the above formulation, a computer program SIPSR for the analysis of the transient state of the binary system[1] was modified to deal with the three-component system. The difference in the estimates between the non-SPR and the MSPR models is discussed in a later section.

EXPERIMENTAL

A 32-channel UV-photometric detector was used to observe the transient isotachopherogram[5]. The 32 photometric cells with photodiode detectors were arrayed along the separation tube at intervals of *ca.* 5 mm (16.6 cm/32 channels). Quartz optical fibres were used to pass UV light from a deuterium lamp to the tube. The UV light from each lamp was passed through an UV-glass filter (Toshiba Glass, Tokyo, Japan; Model D33S, λ_{max} = 330 nm). A single cycle to scan the 32 detectors required *ca.* 0.25 s, and the speed was sufficiently high to trace the variation of the zone lengths accurately. For the data acquisition, an NEC PC9801E microcomputer was used (Tokyo, Japan). The separating tube (polychlorofluoroethylene) was 0.51 mm I.D. and 1 mm O.D. All experiments were carried at 25°C.

The samples were SPADNS, MCA and PIC. Except for MCA, these samples absorb visible and UV light. The sodium salt of SPADNS was obtained from Dojin in the most pure form. The others were obtained from Tokyo Kasei (extra pure grade).

The concentration of the leading electrolyte (HCl) was 5 m*M*. The pH was adjusted to 3.6 by adding β-alanine. The terminator was 10 m*M* caproic acid. Hydroxypropylcellulose (HPC, 0.2%) was added to the leading and terminating electrolytes to suppress electroendosmosis. The viscosity of the 2% aqueous solution is 1000–4000 cps at 20°C according to the specification. The sample solution was injected

into the terminating electrolyte near the boundary between the leading and the terminating electrolytes. The pH of the terminating electrolyte was also adjusted by β-alanine to ensure the pH of the sample solution at the initial stage of migration was equal to the prepared value. The pH measurements were carried using a Model F7ss expanded pH meter (Horiba, Tokyo, Japan).

The data processing and the simulation were performed by the use of an NEC PC9801VX microcomputer.

RESULTS AND DISCUSSION

Under the electrolyte conditions used, the samples were detected in the order of SPADNS, MCA and PIC. The simulated effective mobilities, m, at the steady state were $47.7 \cdot 10^{-5}$, $35.1 \cdot 10^{-5}$, and $29.3 \cdot 10^{-5}$ cm^2 V^{-1} s^{-1}, and the R_E values ($R_E = \bar{m}_L/\bar{m}_S = E_S/E_L$, where E = the potential gradient and L and S are the leading and sample ions) were 1.59, 2.16 and 2.59 respectively. Table I shows the m_0 and pK_a values of the samples and electrolyte constituents used in the simulations.

The mobility and pK_a values of SPADNS were obtained by the isotachophoretic method. The pK_a value of the trivalent anion was rather high considering the chemical structure, suggesting that ion pairs might be formed between the β-alanine monocation and the SPADNS trianion. However, we treated them as free ions, because the simulated zone lengths and the R_E values agreed well with those observed.

Validity of the transient state models

At first the validity of the models was examined by comparing the observed resolution time with that observed. The sample was an equimolar (1.39 mM) mixture of SPADNS (S), MCA (M) and PIC (P). The pH values of the sample solution (pH$_S$) were 3 and 4.

Fig. 2 shows the evolution of the observed transient isotachopherograms of the SPADNS–MCA–PIC system. The number of data used for the evolution was 2600 (650 s). The pH$_S$ was 3 and the sample amounts were 11.1 (A), 16.7 (B) and 22.2 nmol (C) respectively. In Fig. 2, the boundaries between the leading and SPADNS zones

TABLE I

PHYSICO-CHEMICAL CONSTANTS USED IN SIMULATION (25°C)

m_0 = Absolute mobility (cm^2 V^{-1} s^{-1}) $\cdot 10^5$; pK_a = thermodynamic acid dissociation constant; assumed values being used for Cl^-, $SPADNS^-$ and $SPADNS^{2-}$.

Ions	m_0	pK_a
Cl^-	79.08	−2
β-Alanine$^+$	36.7[a]	3.552
$SPADNS^-$	21.0	−3
$SPADNS^{2-}$	42.0	−2
$SPADNS^{3-}$	63.0	3.55
Monochloroacetate$^-$	41.1[a]	2.865
Picrate$^-$	31.5	0.708

[a] The mobilities were obtained by our isotachophoretic method or conductivity measurement. The other mobilities and pK_a values are taken from ref. 9.

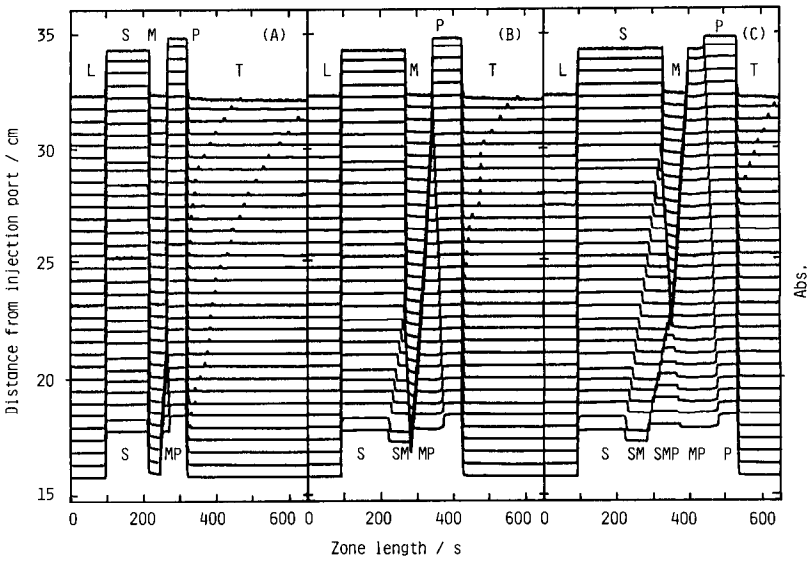

Fig. 2. Transient isotachopherogram of SPADNS(S), monochloroacetic acid (M) and picric acid (P) observed by the use of a 32-channel UV-photometric detector. The sample concentration was 1.39 m*M* and the pH was 3. The sample amounts were 11.1 (A), 16.7 (B) and 22.2 nmol (C). The positions of the baselines of the UV absorption show the distance of the photocell from the sample injection port. The migration current was 49.2 μA. The leading electrolyte was 5 m*M* HCl and the pH was adjusted to 3.6 (buffer: β-alanine). The terminator was 10 m*M* caproic acid.

have been rearranged at the same abscissa position to demonstrate clearly the change in the individual zone lengths at the transient state. The observed overall time-based zone lengths were 222.8, 332.4 and 439.8 s respectively. In Fig. 2A, the mixed zone observed was only that of MCA and PIC (MP). In Fig. 2B the SPADNS–MCA mixed zone (SM) was observed too, and in Fig. 2C the SPADNS–MCA–PIC mixed zone (SMP) was observed in addition to them. The cause of the small peaks in the terminating zone was not apparent.

In order to determine the boundary detection time and subsequently the boundary velocity, the observed UV signals in Fig. 2 were differentiated with respect to time. From the data number at the resultant positive and negative peaks and the sampling rate, the boundary detection time was obtained. The boundary functions were determined by the linear least-squares method on the basis of the boundary detection time and the exact position of each detector. The resolution time was obtained by solving simultaneous boundary equations. For example, the boundary functions of S/SM and SM/S were used to obtain $t_{res,SM}$. For the evaluation of $t_{res,SMP}$, the boundary functions for SM/M and M/MP were used together with those of SM/SMP and SMP/MP. They coincided within 10 s and the average was used for $t_{res,ABC}$. The probable error of the evaluated t_{res} was *ca.* 10 s.

Fig. 3 shows t_{res} *vs.* the time-based whole zone length at $pH_S = 3$ and 4 for the mixed zones SM, MP and SMP. Apparently $t_{res,MP}$ depended on pH_S. On the other hand, the pH_S dependence of $t_{res,SM}$ and $t_{res,SMP}$ was slight. The best-fitted linear functions were as follows:

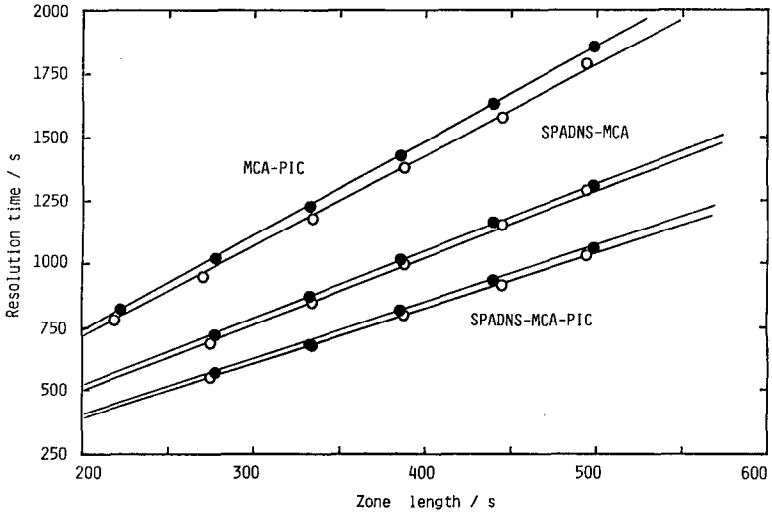

Fig. 3. The observed resolution time *vs.* the whole zone length in the SPADNS–monochloroacetic acid–picric acid system. pH_S 3 (⅛) and 4 (@). For the operating system, see Fig. 1. The sample amounts were 11.1, 13.9, 16.7, 19.5, 22.2 and 25.0 nmol, respectively.

$$\begin{array}{lllll} \text{SMP} & t_{res} = 2.13\ t_{zone} - 8.7 & pH_S = 3.0 \\ & t_{res} = 2.08\ t_{zone} - 8.0 & pH_S = 4.0 \\ \text{SM} & t_{res} = 2.63\ t_{zone} - 2.7 & pH_S = 3.0 \\ & t_{res} = 2.60\ t_{zone} - 10.8 & pH_S = 4.0 \\ \text{MP} & t_{res} = 3.72\ t_{zone} - 4.7 & pH_S = 3.0 \\ & t_{res} = 3.59\ t_{zone} - 9.0 & pH_S = 4.0 \end{array} \quad (65)$$

where t_{zone} is the time-based zone length of the whole sample. The pH_S dependence of $t_{res,MP}$ was *ca.* 4% over the pH range studied.

Table II shows the observed and simulated resolution times and the separation numbers. For simulation, both the non-SPR and the MSPR models were used. The separation number, which correlates with the amount of sample separable per unit time, was defined as follows[2]:

$$S = \frac{F}{i} \cdot \frac{\partial n_A}{\partial t} = \frac{F}{i} \cdot \frac{n_A}{t_{res}} \quad (66)$$

where F is the Faraday constant, i the migration current and n_A the sample amount of constituent A. The slight pH dependence of $t_{res,MP}$ was simulated by the MSPR model. Good agreement between the observed and the simulated t_{res} was obtained, confirming the validity of this model. Although the observed small pH dependence was not simulated by the non-SPR model, the approximation used in this model is rather good because the discrepancy between the observed and the simulated t_{res} was small. Table III summarizes the pH_S dependence of the observed and simulated boundary velocities. The agreement was satisfactory.

In our previous work on the binary system MCA–PIC (1:1)[1], the separation

TABLE II

SIMULATED AND OBSERVED SEPARATION NUMBERS AND RESOLUTION TIMES FOR THE SPADNS–MONOCHLOROACETATE–PICRATE SYSTEM (1:1:1)

Operational system: leading electrolyte 5 m*M* HCl–β-alanine (pH 3.60); current 49.2 μA; diameter of the separation tube 0.51 mm; sample amount 25 nmol. *S* = Separation number, see text; t_{res} = resolution time; sim = simulated; obs = observed.

pH_S	*SMP*			*SM*			*MP*		
	sim		*obs.*[a]	*sim*		*obs.*	*sim*		*obs.*
	Non-SPR	*MSPR*		*Non-SPR*	*MSPR*		*Non-SPR*	*MSPR*	
Resolution time (s)									
3	1037	1040	1049	1258	1286 (1186)[b]	1304	1788	1808 (1367)	1843
4	–	1037	1025	–	1293 (1214)	1281	–	1765 (1279)	1774
Separation number									
3				0.0390	0.0381 (0.0413)	0.0377 ±0.0001	0.0274	0.0271 (0.0359)	0.0266 ±0.0001
4				–	0.0379 (0.0404)	0.0383 ±0.0003	–	0.0278 (0.0383)	0.0279 ±0.0004

[a] The probable error for t_{res} was *ca.* 10 s.
[b] The values in parentheses are the estimates when the simulation was carried out for the binary systems.

TABLE III

SIMULATED AND OBSERVED RELATIVE BOUNDARY VELOCITY AT pH_S = 3 AND 4

For the electrolyte systems, see Table II. V_R = relative boundary velocity, $V_{boundary}/V_{IP}$.

	V_R		
	Non-SPR	*MSPR*	*obs*
pH_S = 3			
SM/SMP	0.713	0.710	0.724 ± 0.002
SMP/MP	1.210	1.204	1.154 ± 0.004
S/SM	0.784	0.788	0.799 ± 0.003
SM/M	1.117	1.121	1.102 ± 0.012
M/MP	0.886	0.894	0.891 ± 0.002
MP/P	1.074	1.073	1.068 ± 0.005
pH_S = 4			
SM/SMP	0.713	0.708	0.720 ± 0.005
SMP/MP	1.210	1.201	1.150 ± 0.007
S/SM	0.784	0.790	0.795 ± 0.001
SM/M	1.117	1.122	1.101 ± 0.004
M/MP	0.886	0.890	0.881 ± 0.006
MP/P	1.074	1.068	1.053 ± 0.006

number decreased with decreasing pH_S. A similar tendency was found in the SPADNS–MCA–PIC system (1:1:1).

Table IV shows the simulated R_E values, effective mobilities and concentrations of the zone constituents of the SPADNS–MCA–PIC system at both the steady state and the transient state. The difference in these estimates between the models used was significant for the sample concentrations in the mixed zone.

Difference in separation capacity between the two- and three-component systems

The resolution time of adjacent samples in multi-component systems is larger than that of the binary system even if the amount of each component is the same. In this section the cause of this difference is discussed.

TABLE IV

SIMULATED R_E VALUES, EFFECTIVE MOBILITIES AND CONCENTRATIONS IN THE STEADY AND TRANSIENT ZONES OF THE SPADNS–MONOCHLOROACETATE–PICRATE SYSTEM AT pH_L = 3.6 (25°C)

R_E = Ratio of potential gradients, $E_{zone}/E_{leading}$; $\bar{m}_S$, $\bar{m}_M$ and $\bar{m}_P$ = effective mobilities of SPADNS(S), monochloroacetate (M) and picrate ions (P) ($cm^2\ V^{-1}\ s^{-1}$) · 10^5; pH = pH of zones at the steady and transient states; C^t_S, C^t_M and C^t_P = total concentrations of samples (m*M*); C^t_Q = total concentration (m*M*) of buffer (β-Ala); $\bar{m}_Q$ = effective mobility of buffer ($cm^2\ V^{-1}\ s^{-1}$) · 10^5; I = ionic strength · 10^3.

Zone	R_E	*pH*	$\bar{m}_S$	$\bar{m}_M$	$\bar{m}_P$	C^t_S	C^t_M	C^t_P	$\bar{m}_Q$	C^t_Q	I
Steady state zone											
S	1.597	3.721	47.5	–	–	1.500	–	–	14.3	9.07	7.66
M	2.153	3.820	–	35.2	–	–	3.669	–	12.6	8.69	3.32
P	2.574	3.840	–	–	29.5	–	–	3.096	12.3	8.33	3.09
Transient zones, three-component system Non-SPR model[a]											
SMP	1.875	3.771	48.9	34.4	28.9	0.791	0.791	0.791	13.4	8.79	5.57
SM	1.760	3.717	48.1	33.8	–	0.974	1.521	–	14.4	8.86	6.29
MP	2.282	3.877	–	35.7	29.5	–	2.095	1.215	11.6	8.96	3.13
MSPR model[a] pH_S = 3											
SMP	1.868	3.769	48.9	34.4	28.8	0.793	0.785	0.813	13.5	8.81	5.59
SM	1.752	3.756	48.5	34.2	–	0.954	1.353	–	13.7	8.94	6.10
MP	2.305	3.827	–	35.3	29.4	–	2.140	1.295	12.5	8.55	3.24
MSPR model[a] pH_S = 4											
SMP	1.862	3.768	48.9	34.4	28.8	0.797	0.828	0.767	13.5	8.82	5.60
SM	1.754	3.756	48.6	34.2	–	0.948	1.368	–	13.7	8.94	6.08
MP	2.295	3.826	–	35.3	29.4	–	2.232	1.218	12.5	8.56	3.24
Transient zones, two-component system Non-SPR model[a]											
SM	1.716	3.748	48.3	34.0	–	1.070	1.070	–	13.8	8.97	6.43
MP	2.360	3.830	–	35.3	29.4	–	1.679	1.679	12.4	8.50	3.20
MSPR model[a] pH_S = 3											
SM	1.718	3.749	48.3	34.1	–	1.063	1.087	–	13.8	8.97	6.41
MP	2.368	3.830	–	35.3	29.4	–	1.617	1.731	12.4	8.49	3.20
MSPR model[a] pH_S = 4											
SM	1.728	3.751	48.4	34.1	–	1.030	1.167	–	13.8	8.96	6.32
MP	2.353	3.830	–	35.3	29.4	–	1.741	1.626	12.4	8.50	3.21

[a] For the definitions of the transient state models, see text.

The equimolar SPADNS–MCA–PIC, SPADNS–MCA and MCA–PIC systems were analyzed by the MSPR model. The sample amount was 25 nmol, the leading electrolyte was 5 m*M* HCl buffered by β-alanine (pH 3.6), the capillary diameter was 0.5 mm and the migration current was 50 μA. Fig. 4 shows the pH_S dependence of the sample concentration in the mixed zones simulated by the MSPR model (A = SPADNS–MCA–PIC, B = SPADNS–MCA and C = MCA–PIC). Mixed zones with the same constituents are formed in the two- and three-component systems. To distinguish, for example, the SPADNS–MCA mixed zone formed in the three-component system from that formed in the two-component system, the former was abbreviated as SM(3) and the latter as SM(2). From Fig. 4B and C, the concentrations of the sample constituents in the mixed zones SM(2) and MP(2) were similar to each other when the samples were equimolar. In the SMP zone, the concentrations of the sample constituents were also very similar. On the other hand, a remarkable difference was found between the concentrations of SPADNS and MCA in the SM(3) zone. A similar situation was found for the concentrations of MCA and PIC in the MP(3) zone. The concentrations of the individual samples in the SM(2) and MP(2) zones were split into lower and higher values in the SM(3) and MP(3) zones. It should be noted that the abundance of the more mobile component SPADNS in the SM(3) zone is smaller than that in the SM(2) zone, and the abundance of the more mobile component MCA in the MP(3) zone is larger than that in the SM(2) zone. This phenomena was decisive in elucidating the decrease in the separation capacity in the three-component system. We call this the concentration splitting hereafter.

Fig. 5A shows the pH_S dependence of the R_E values ($E_{\text{mixed zones}}/E_{\text{leading zone}}$) of the mixed zones simulated by the MSPR model. From Fig. 5A the following relationship among the potential gradients, *E*, of the mixed zones is valid:

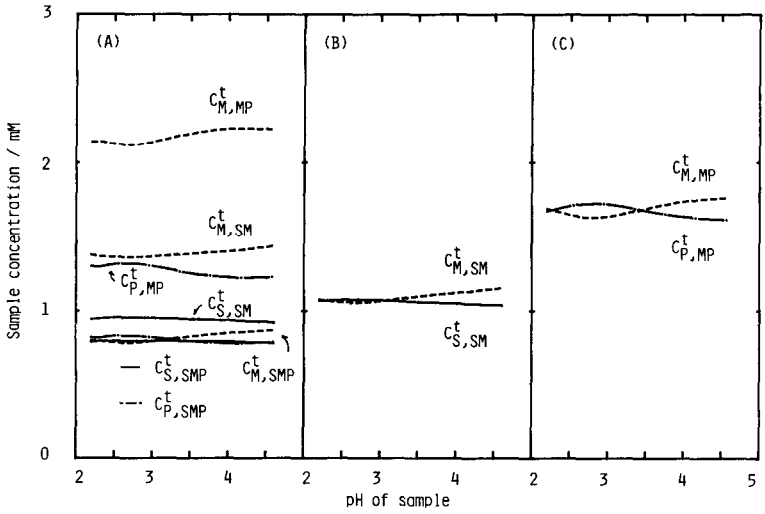

Fig. 4. The pH_S dependence of the sample concentration in the mixed zones simulated by the MSPR model. (A) SPADNS–MCA–PIC equimolar system, (B) SPADNS–MCA equimolar system, (C) MCA–PIC equimolar system. C^t = Total concentration of the sample. The subscripts SMP, SM and MP represent the mixed zones of SPADNS–MCA–PIC, SPADNS–MCA and MCA–PIC. For the operating system, see Fig. 1. The migration current was 50 μA and the I.D. of the separating tube was 0.5 mm.

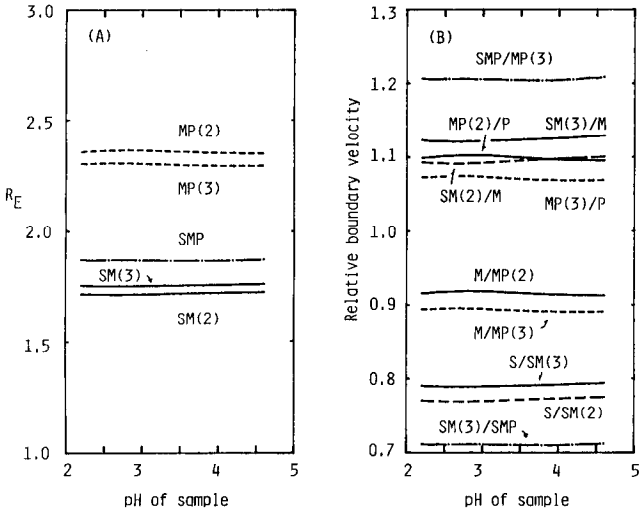

Fig. 5. (A) The pH_S dependence of the R_E values of the mixed zones formed in the SPADNS–MCA–PIC, SPADNS–MCA and MCA–PIC equimolar systems. (B) The pH_S dependence of the relative boundary velocities (boundary velocity/isotachophoretic velocity). Figures in parentheses show the number of components in the sample solution. For the operating system, see Fig. 1. The migration current was 50 μA and the I.D. of the separating tube was 0.5 mm.

$$E_{SM(2)} < E_{SM(3)} \tag{67}$$

$$E_{MP(3)} < E_{MP(2)}$$

Since the pH values of the mixed zones of SM(2) and SM(3) as well as of the MP(2) and MP(3) zones were very similar, the main cause of the above relationship was attributed to the concentration splitting.

Fig. 5B shows the pH_S dependence of the relative boundary velocities, $V_{boundary}/V_{IP}$. The boundary velocities were expressed by eqns. 11–16. From Fig. 5B, the following relationship is valid:

$$V_{R,S/SM(2)} < V_{R,S/SM(3)} < 1 < V_{R,SM(2)/M} < V_{R,SM(3)/M}$$
$$V_{R,M/MP(3)} < V_{R,M/MP(2)} < 1 < V_{R,MP(3)/P} < V_{R,MP(2)/P} \tag{68}$$

From the above relationship and eqns. 27 and 33 for $t_{res,SM}$ and $t_{res,MP}$, one can easily estimate the following result:

$$t_{res,SM(2)} < t_{res,SM(3)} \tag{69}$$

$$t_{res,MP(2)} < t_{res,MP(3)}$$

The $t_{res,MP(3)}$ should be evaluated by the use of eqn. 64, however, the use of the approximation of eqn. 33 is more straightforward for the present situation.

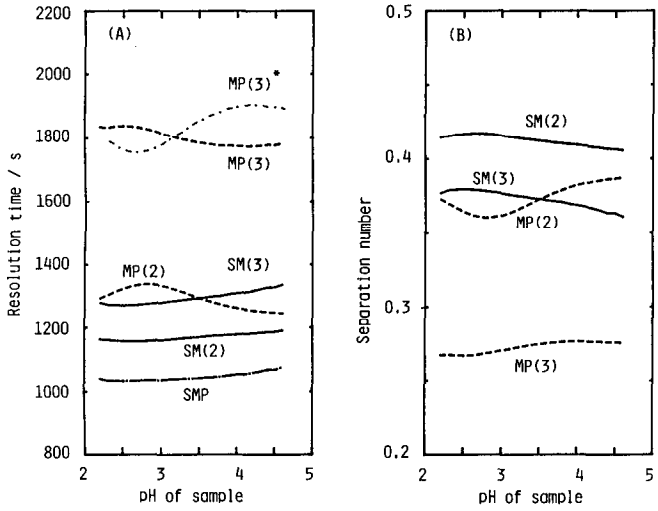

Fig. 6. The pH_S dependence of t_{res} (A) and the separation number (B) in the SPADNS–MCA–PIC, SPADNS–MCA and MCA–PIC equimolar systems. For the operating system, see Fig. 1. The migration current was 50 μA and the I.D. of the separating tube was 0.5 mm.

Fig. 6A and B show the pH_S dependence of t_{res} and the separation number (eqn. 66) simulated by the MSPR model. The relationships 69 were valid. In Fig. 6A, $t_{res,MP(3)}^*$ was evaluated by use of eqn. 33. Apparently, the pH_S dependence of $t_{res,MP(3)}^*$ was in conflict with observation, suggesting that the approximation of the non-SPR approach is not accurate.

Thus the separation process of the three-component system and the decrease in the separation capacity in comparison with the binary system was elucidated exactly by the MSPR model. Although the pH_S dependence was simulated only by the MSPR model, at least for the present samples, the non-SPR model was useful for the approximate evaluation of t_{res}.

As described, the iteration calculations in the MSPR approach to the self-consistent state were rather complex, and time-consuming. The time needed for the non-SPR approach for the analysis of the present three-component system was 11 s by the use of microcomputers equipped with a CPU i80286 (clock 8 MHz; part of the calculation was performed with a coprocessor i80287). However, it took 80 s when the MSPR model was used. Beside the transient state simulation, it took 15 s for the steady state analysis. The selective use of these models may be adequate for the purpose of the simulation.

ACKNOWLEDGEMENTS

One of the authors (T.H.) thank the Ministry of Education, Science, and Culture of Japan for support of part of this work under a Grant-in-Aid for Scientific Research (No. 61540423).

REFERENCES

1 T. Hirokawa, K. Nakahara and Y. Kiso, *J. Chromatogr.*, 463 (1989) 51.
2 F. E. P. Mikkers, F. M. Everaerts and J. A. F. Peek, *J. Chromatogr.*, 168 (1979) 293.
3 F. E. P. Mikkers, F. M. Everaerts and J. A. F. Peek, *J. Chromatogr.*, 168 (1979) 317.
4 G. Brouwer and G. A. Postema, *J. Electrochem. Soc.*, 117 (1970) 874.
5 T. Hirokawa, K. Nakahara and Y. Kiso, *J. Chromatogr.*, 463 (1989) 39.
6 R. A. Alberty, *J. Am. Chem. Soc.*, 72 (1950) 2361.
7 F. M. Everaerts, J. L. Beckers and Th. P. E. M. Verheggen, *Isotachophoresis*, Elsevier, Amsterdam, 1976.
8 T. Hirokawa, M. Nishino, N. Aoki, Y. Kiso, Y. Sawamoto, T. Yagi and J.-I. Akiyama, *J. Chromatogr.*, 271 (1983) D1.
9 R. A. Robinson and R. H. Stokes, *Electrolyte Solutions*, Butterworths, London, 1959.